Journal of Environmental Science and Engineering A 15 (2026) 31-39
doi:10.17265/2162-5298/2026.01.004

Winter 3D T-S-ρ Structures and Dispersion of Thermal Discharge near Tianwan NPP

Yutao Cheng[1], Xiaotian Dong[1], Hongya Lu[2], Guochang Sun[3], Jian Wang[1] and Weicheng Lv[1]

1. Jiangsu Ocean University, Lianyungang 222005, China

2. Lianyungang Water Resources Planning and Design Institute Co., Ltd., Lianyungang 210007, China

3. Lianyun District Bureau of Agriculture and Rural Affairs, Lianyungang 222043, China

Abstract: A mathematical model of thermal effluent dispersion was developed for the TNPP (Tianwan Nuclear Power Plant) and rigorously validated against available observations. Using the validated model, the spatial extent of the 1-4 °C temperature-rise zone was quantified, and the temperature field characteristics in plan view, along vertical sections, and along water columns were systematically investigated. The results show that the vertical temperature gradient ranges from -0.34 to 1.10 °C m^{-1}. The gradient increases toward the outfall; specifically, the tidally averaged water-column temperature gradient decreases from 0.18 °C m^{-1} at Station 3# to 0.08 °C m^{-1} at Station 14#. Vertical mixing is stronger during spring tides, whereas during neap tides the tidally averaged water-column temperature gradient is higher than that during spring tides by 0.02-0.17 °C m^{-1}. Along the dominant transport pathway, the tidally averaged horizontal (along-path) temperature gradient is approximately 0.88-1.02 °C km^{-1}.

Key words: Thermal discharge, water temperature distribution, salinity distribution, density distribution, three-dimensional dispersion, marine ecology.

1. Introduction

Nuclear power, as an efficient, reliable, and low-carbon source of electricity, plays an important role in ensuring energy security, addressing climate change, and promoting sustainable development [1]. Nevertheless, the discharge of waste heat from nuclear power plants produces thermal effluents that can alter the hydrodynamic environment and ecological conditions of adjacent coastal waters [2-7]. Understanding the spatiotemporal patterns of temperature distribution is therefore essential for assessing marine environmental impacts, optimizing discharge strategies, and safeguarding the ecological security of nearby seas. In particular, thermal discharges can modify local seawater temperature fields, thereby affecting seawater density, hydrodynamic processes, material transport, and marine ecosystems. Accurate prediction of the thermal plume extent and a detailed characterization of temperature distributions in the horizontal, vertical, and cross-sectional directions are of great significance.

To date, extensive research on thermal discharges from power plants has been conducted worldwide using numerical simulations, physical experiments, and field observations. Arieli et al. deployed monitoring stations along the direction of temperature decay in the coastal waters near the Hadera power plant, obtained temperature distributions, and further investigated the effects of temperature elevation on phytoplankton [8]. Zeng et al. combined numerical modeling with in situ observations to examine the influence of thermal effluents on surrounding waters, showing that the impact was largely confined to the surface layer and decreased with increasing water depth [9]. Lowe et al. developed a mathematical model to study thermal plume dispersion in estuarine environments and reported that plume dynamics dominated the diffusion process [10]. Tang employed AVHRR (Advanced Very

Corresponding author: Xiaotian Dong, Ph.D., research fields: port, coastal and offshore engineering.

High Resolution Radiometer) sea surface temperature data with a spatial resolution of 9 km to evaluate the influence of the Daya Bay Nuclear Power Station on sea surface temperature [11]. Using MIKE3, Pan et al. investigated thermal discharge in Sanmen Bay and found that temperature elevation was transported primarily along the main tidal current direction; high-temperature anomalies were concentrated near the outfall, whereas lower-temperature increases spread laterally, with a markedly larger affected area in winter than in summer [12].

Because seawater density varies with temperature, pronounced vertical stratification often develops in the vicinity of the outfall [13]. Consequently, a three-dimensional hydrodynamic model is indispensable for accurately resolving the thermal structure in the receiving waters [14, 15]. The receiving area of the TNPP (Tianwan Nuclear Power Plant) is located within a semi-enclosed bay formed by the Lianyun District coastline and the Xuwei breakwater, where water exchange is relatively weak. Heat accumulation in such a setting may further modify the local marine ecological environment. In this study, the receiving waters of the Tianwan Nuclear Power Plant are selected as the study area. Based on thorough model calibration and validation, we predict the characteristics of the thermal discharge and analyze the horizontal, vertical, and cross-sectional distributions of seawater temperature, thereby providing scientific support for marine ecological and environmental protection.

2. Study Area and Mesh Generation

The TNPP (Tianwan Nuclear Power Plant) is located in the Lianyun District of Lianyungang, Jiangsu Province, China (Fig. 1). Cooling-water discharges from each phase adopt an integrated engineering scheme consisting of a culvert, a dredged deep outlet channel excavated on the seabed, and a training (guide) dike. The training dike extends from the northern dike of the discharge outlet for Units 1-2, turns toward the southwest along a 60° circular arc with a length of 522 m, and then continues as a straight segment of 694 m. This configuration consolidates the discharges from Phase I and the expansion project and guides the combined flow southeastward along the coastline. Under full-power operation, the total discharge rate is approximately 500 m³/s, with about 100 m³/s from Outfall 1 and 400 m³/s from Outfall 2 (Fig. 1); the temperature rise of the discharged water is

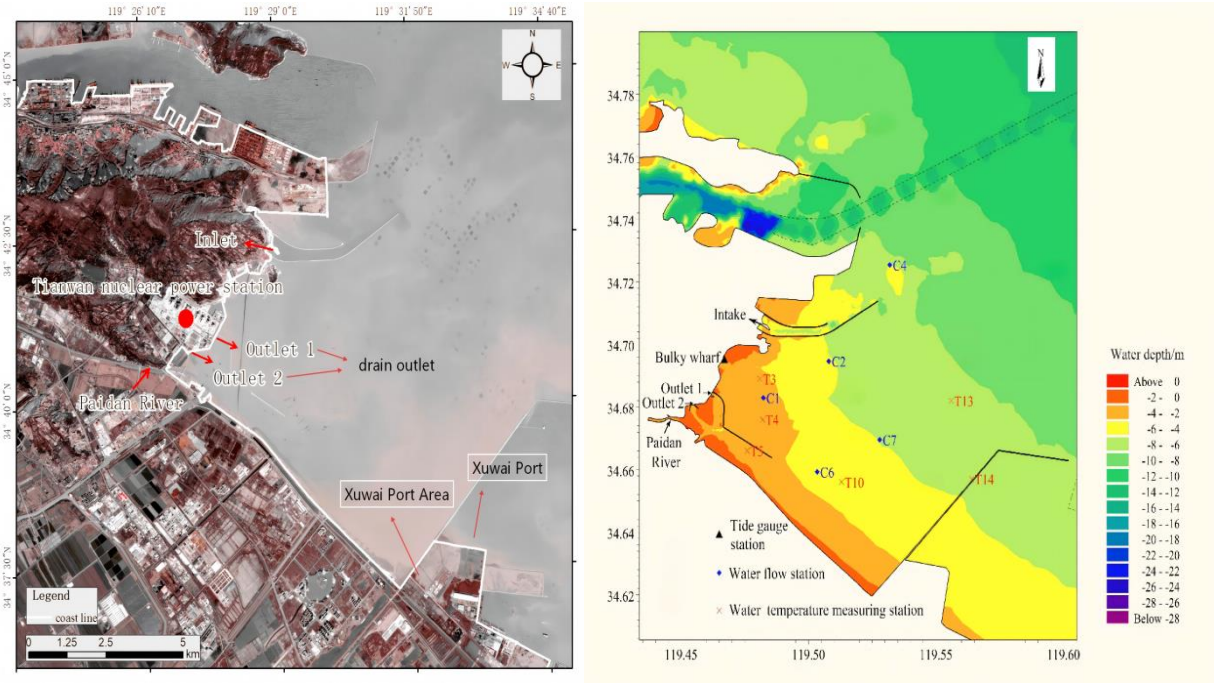

Fig. 1 Location of the study area and monitoring stations.

10 °C for both outfalls. Such a large discharge and temperature elevation may generate a distinct thermal plume in the nearshore waters, making accurate representation of the outfall geometry and local bathymetry important for subsequent simulations.

Tidal currents in the study area are primarily controlled by offshore tidal forcing. Therefore, a South Yellow Sea tidal-current model covering the entire Lianyungang coastal waters was employed. An unstructured triangular mesh was generated with local refinement in the study area, particularly around the outfalls and nearshore zone, to better capture sharp gradients in flow and temperature. The final grid comprises 24,363 elements and 12,933 nodes, with a minimum mesh resolution of 5 m. This locally refined mesh provides sufficient detail to resolve near-field circulation while maintaining an efficient representation of regional tidal dynamics.

3. Development of the Three-Dimensional Hydrodynamic Model

3.1 Governing Equations

The three-dimensional tidal-current model is formulated based on the continuity equation and the momentum equations, which are given as follows.

Continuity equation:

$$\frac{\partial u}{\partial x}+\frac{\partial v}{\partial y}+\frac{\partial w}{\partial z}=S \tag{1}$$

Momentum equations:

$$\frac{\partial u}{\partial t}+u\frac{\partial u}{\partial x}+v\frac{\partial u}{\partial y}+w\frac{\partial u}{\partial z}-fv=-\frac{1}{\rho}\frac{\partial P}{\partial x}+\frac{\partial}{\partial x}\left(E\frac{\partial u}{\partial x}\right)+\frac{\partial}{\partial y}\left(E\frac{\partial u}{\partial y}\right)+\frac{\partial}{\partial z}\left(E\frac{\partial u}{\partial z}\right)+u_sS \tag{2}$$

$$\frac{\partial v}{\partial t}+u\frac{\partial v}{\partial x}+v\frac{\partial v}{\partial y}+w\frac{\partial v}{\partial z}+fu=-\frac{1}{\rho}\frac{\partial P}{\partial y}+\frac{\partial}{\partial x}\left(E\frac{\partial v}{\partial x}\right)+\frac{\partial}{\partial y}\left(E\frac{\partial v}{\partial y}\right)+\frac{\partial}{\partial z}\left(E\frac{\partial v}{\partial z}\right)+v_sS \tag{3}$$

$$\frac{\partial w}{\partial t}+u\frac{\partial w}{\partial x}+v\frac{\partial w}{\partial y}+w\frac{\partial w}{\partial z}=-\frac{1}{\rho}\frac{\partial P}{\partial z}+\frac{\partial}{\partial x}\left(E\frac{\partial w}{\partial x}\right)+\frac{\partial}{\partial y}\left(E\frac{\partial w}{\partial y}\right)+\frac{\partial}{\partial z}\left(E\frac{\partial w}{\partial z}\right)-g+w_sS \tag{4}$$

$$\frac{\partial \Delta T}{\partial t}+u\frac{\partial \Delta T}{\partial x}+v\frac{\partial \Delta T}{\partial y}+w\frac{\partial \Delta T}{\partial z}=\frac{\partial}{\partial x}\left(D\frac{\partial \Delta T}{\partial x}\right)+\frac{\partial}{\partial y}\left(D\frac{\partial \Delta T}{\partial y}\right)+\frac{\partial}{\partial z}\left(D\frac{\partial \Delta T}{\partial z}\right)-\frac{K_s\Delta T}{\rho c_p(h+\zeta)}+\Delta T_sS \tag{5}$$

where: t is time (s); h is the total water depth (m); ζ is the water level relative to the xoy coordinate plane (m); u, v, and w are the velocity components in the x-, y-, and z-directions, respectively (m/s); f is the Coriolis parameter($f = 2\omega\sin\varphi$, ω is the Earth's angular rotation rate, and φ is latitude); ρ is density (kg/m^3); P is pressure (Pa); and E is the generalized (eddy) diffusion coefficient for momentum (m^2/s). S denotes the source/sink term; u_s,v_s, and w_s are the velocity components of the source term in the x-, y-, and z-directions, respectively (m/s). ΔT is the temperature anomaly (℃); T is water temperature (℃); and T∞ is the ambient (natural) water temperature (℃), with $\Delta T = T - T\infty$. D is the generalized diffusion coefficient for scalar transport; ΔT_s is the temperature anomaly associated with the source term (℃); and K_s is the integrated surface heat-loss coefficient.

3.2 Initial and Boundary Conditions

In the model, the initial conditions are set to zero, and the influence of the initial-value error gradually diminishes after a spin-up period. In the vertical direction, all flow variables are set to zero at land boundaries. For the offshore open boundary, the tidal elevation time series derived from harmonic tidal prediction is prescribed. For the TNPP discharge boundaries, the flow rates are specified as 100 m³/s for Outfall 1 and 400 m³/s for Outfall 2. A wetting-drying scheme is employed to define the moving boundary of tidal flats that are intermittently inundated and exposed, thereby representing the wetting and drying processes.

Within the computational domain, the initial temperature anomaly is set to zero, and an adiabatic condition is imposed along the shoreline boundary. The

Manning roughness coefficient n is taken in the range 0.0125-0.04. The generalized (eddy) diffusion coefficient for momentum E is set within 0.1-5 m²/s. Because TNPP is located near 35°N, the Coriolis parameter is approximated as $f' \approx 8.3 \times 10^{-5}$ s^{-1}. Based on local winter meteorological and hydrothermal conditions in the vicinity of the study area (mean water temperature 2.6 °C, mean air temperature 3.0 °C, mean atmospheric pressure 1,025 hPa, mean relative humidity 63%, and mean wind speed 5.1 m/s), the integrated surface heat-loss coefficient is calculated as $K_s = 24.0$ W m^{-2} °C^{-1}.

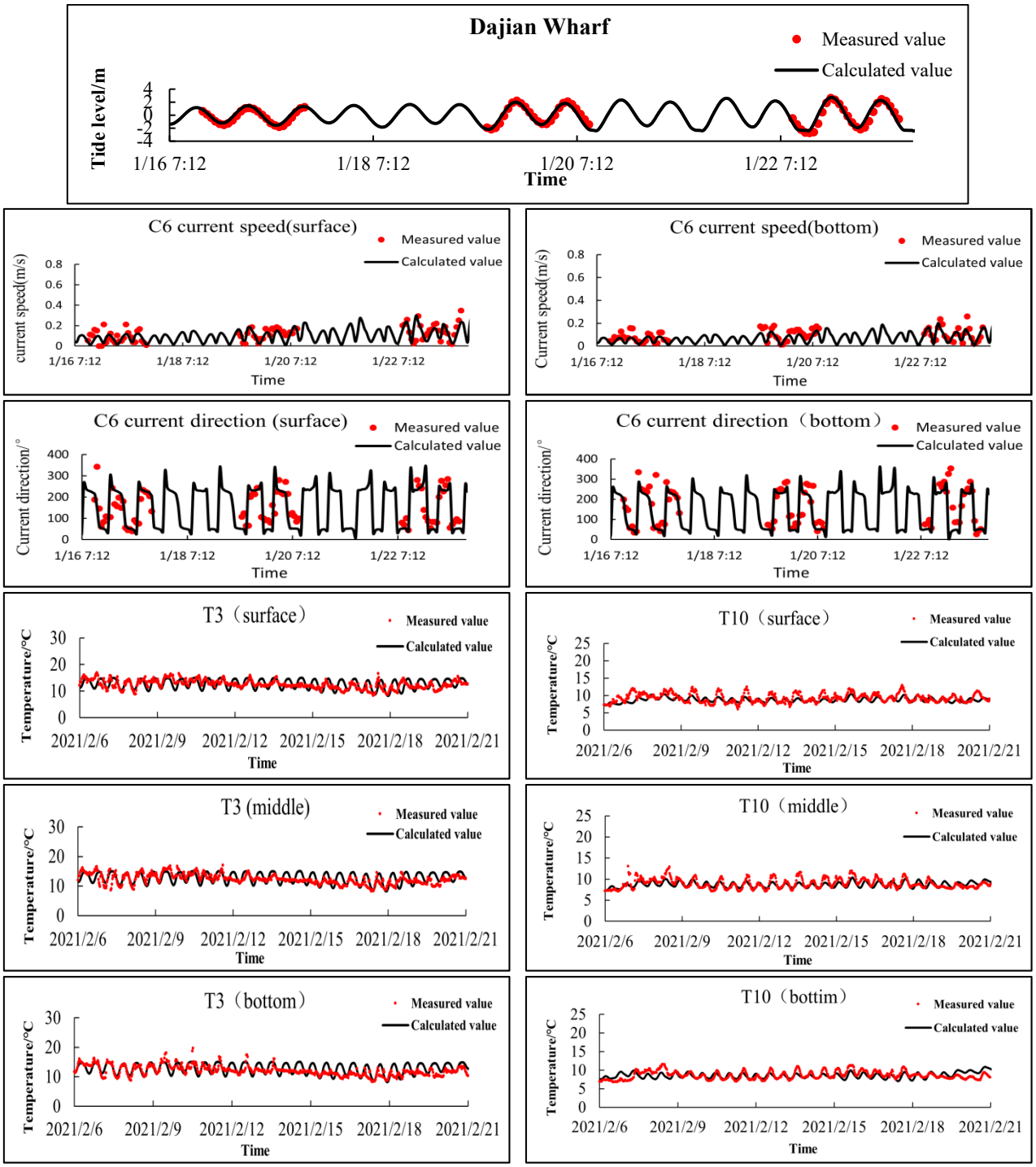

Fig. 2 Validation of water level, current speed and direction, and water temperature.

4. Model Validation

This study collected in situ water temperature measurements from February to March 2021. The observed tidal elevation data at Dajian Wharf were used to validate water levels, while current measurements at stations C6 and C7 were used to validate current speed and direction. Water temperature records at stations T3 and T13 were used for temperature validation (see Fig. 2). The mean error of tidal elevation was 0.03 m, and the mean error of current speed across the tide stations was 0.04 m/s. The mean error of water temperature at station T10 was 0.53 °C. The relatively larger error at station T3 can be attributed to its location in shallow tidal-flat waters, where anomalous sea states (waves and sea ice) and meteorological conditions (precipitation, wind, air humidity, and cloud cover) exert a stronger influence on surface temperature than on bottom temperature. In addition, wetting-drying cycles during flood and ebb tides, together with uncertainties in temperature monitoring, may further increase the discrepancy at T3.

Overall, the validation results indicate good agreement between simulated and observed values. The model reproduces the tidal-current dynamics and temperature conditions in the study area with satisfactory accuracy, demonstrating that the coupled hydrodynamic-temperature model can reliably represent flow motion and thermal variability in the project waters and is suitable for simulating tidal and temperature changes in the study region.

5. Three-Dimensional Distributions and Influencing Factors of Temperature-Salinity-Density Structures along Sections AB and CD

5.1 Section Locations and Scenario Description

To elucidate the vertical structure and along-path spreading and attenuation of the thermal discharge from the Tianwan Nuclear Power Plant in the study area, two representative transects (cross-sections) were selected. The first is Section AB, located near the discharge training dike (approximately 900 m in width), which is used to characterize near-field mixing and sharp-gradient variations in the vicinity of the outfall. The second is Section CD, extending from Yangshan Island toward the western breakwater of Xuwei Port (approximately 8,550 m in width), which is designed to represent mid- to far-field transport and stratification at the bay scale. The spatial relationship of the two sections is shown in Fig. 3.

For the sectional analysis, results at the peak flood stage were selected as the representative time. The "Paitan River discharge scenario" with a flow rate of 523.6 m³/s was applied to output the sectional distributions of temperature, salinity, and density, thereby capturing the three-dimensional structures arising from the combined effects of tidal dynamics and external freshwater inputs. The discharge system of the nuclear power plant adopts a "culvert + dredged deep outlet channel + training dike" configuration that consolidates the effluents and guides the flow southeastward along the coastline. Under full-power operation, the total discharge is approximately 500 m³/s, with a temperature rise of about 10 °C. Under winter

Fig. 3 Locations of cross-Sections AB and CD.

conditions, strong air-sea heat exchange in the study area (integrated surface heat-loss coefficient $K_s \approx 24.0$ W m^{-2} °C^{-1}) plays an important role in controlling far-field thermal attenuation.

5.2 Vertical Temperature Structure and Influencing Factors

As shown in Fig. 4, Section AB exhibits a typical pattern of "rapid near-field attenuation followed by gradual far-field stabilization" along the A→B direction. A high-temperature zone occurs near end A (≈12 °C), where isotherms are tightly packed within 0-300 m and temperature quickly decreases to about 6-7 °C, indicating strong near-field mixing/dilution and concentrated horizontal gradients. Beyond ~400 m, the section enters a low-temperature tail (around the 5.4, 4.8, 4.2, and 3.6 °C isotherms), where isotherm spacing increases and temperature changes become weaker, approaching the ambient background. Vertically, isotherms are nearly upright and the surface-bottom temperature difference at a given location is small, suggesting a well-mixed, quasi "columnar" structure with weak vertical gradients.

As shown in Fig. 4, Section CD displays progressive attenuation at the bay scale together with an evolving vertical structure. A relatively warm region occurs near end C (≈5.6°C), and a localized warm core (≈6.4°C) appears around 1.5-2.2km, implying that the main thermal-transport pathway intersects the section with some lateral offset. Downstream, temperature sequentially crosses the 6.0, 5.2, 4.8, 4.4, 4.0, 3.6, 3.2, and 2.8°C isotherms and approaches the winter background near end D. Compared with AB, the mid-reach of CD shows tilted and curved isotherms, indicating that the temperature field becomes vertically non-uniform in the mid-far field, likely modulated by density stratification (salinity-driven) and tidal dynamics.

Section AB is located in shallow waters near the training dike, where discharge-jet momentum, tidal shear, and bottom friction jointly enhance turbulence and entrainment, leading to rapid dilution over short distances and inhibiting persistent thermal stratification. In contrast, Section CD spans a longer distance and greater depths; the thermal discharge continues to mix with ambient waters during advection. Moreover, strong winter air-sea heat exchange (Ks ≈ 24.0 W m^{-2} °C^{-1}, with relatively high winds) further accelerates far-field cooling, resulting in stepwise attenuation toward the background temperature.

5.3 Vertical Density Structure and Influencing Factors

Density, jointly determined by temperature and salinity, reflects water-mass stability and stratification. In this scenario, the density pattern closely follows salinity, indicating a dominant salinity control, while temperature effects are mainly local.

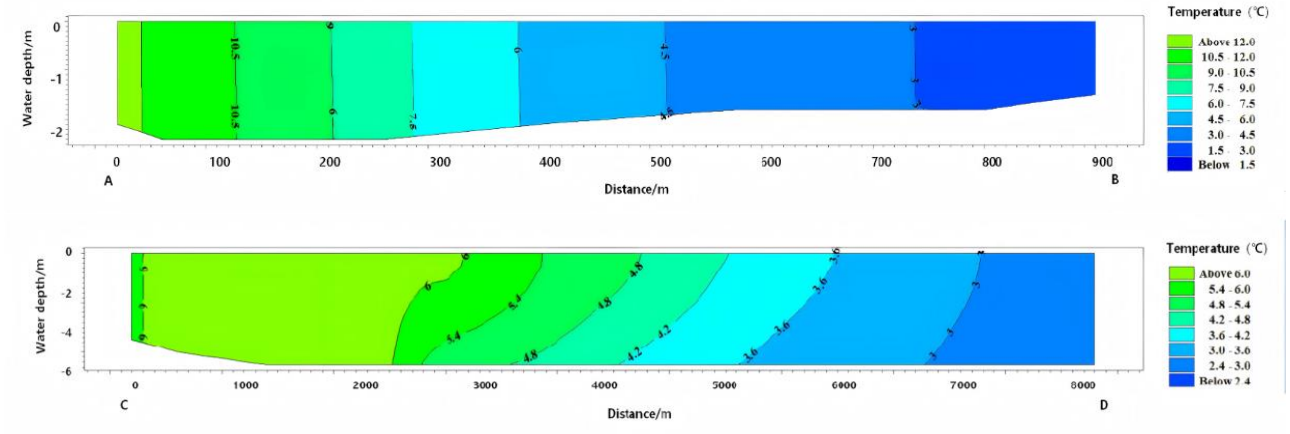

Fig. 4 Vertical temperature distributions along Sections AB and CD (°C).

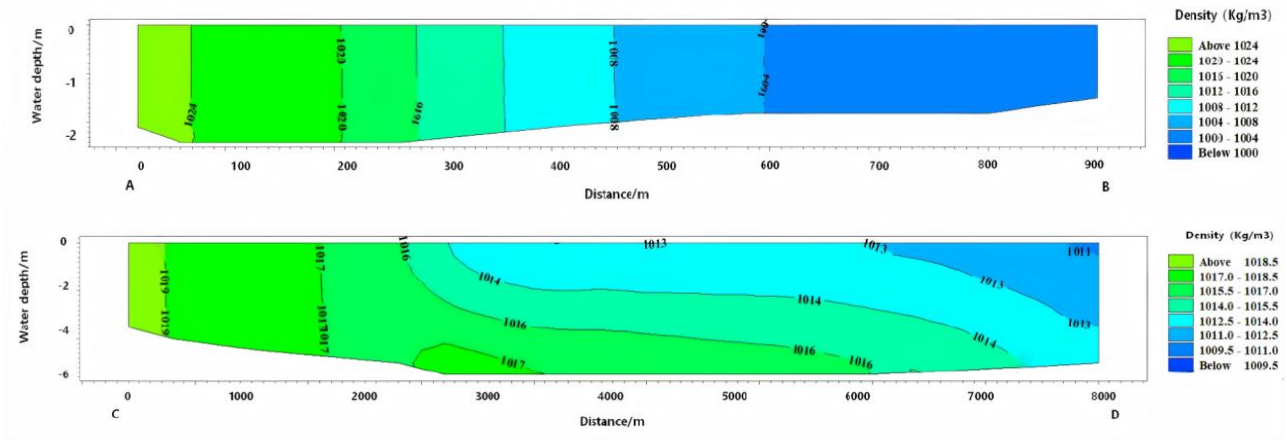

Fig. 5 Vertical density distributions along Sections AB and CD (kg/m³).

As shown in Fig. 5, density along Section AB decreases from ~1,023 kg/m³ near end A to ~1,005-1,002 kg/m³ toward B, with closely spaced isopycnals within ~0-500 m and weak vertical differences, suggesting strong near-field mixing and negligible stratification. Along Section CD, density also declines overall, from ~1,018.8 kg/m³ near C to ~1,012.2-1,011.6 kg/m³ near-surface values toward D. A clear two-layer structure occurs in the mid-reach (~2-7 km), with low-density surface water over a wedge-like high-density bottom layer, consistent with a salt-wedge front.

Overall, freshwater input lowers surface salinity/density and promotes stratification, whereas flood-tide intrusion of dense bottom water helps sustain the two-layer structure in Section CD. Thermal discharge locally reduces density near the outfall but is secondary to salinity-driven effects; shallow AB remains well mixed, while deeper CD allows the pycnocline to persist downstream.

5.4 Vertical Salinity Structure and Influencing Factors

As shown in Fig. 6, salinity along Section AB decreases markedly from A to B, forming a typical horizontal salinity front. Salinity is about 30 near end A and drops rapidly across closely spaced isohalines within ~0-400/500 m, after which the section enters a low-salinity tail where isohalines are more widely spaced and the decrease becomes gradual. Vertically, isohalines are nearly upright and the surface-bottom salinity difference is small, indicating strong vertical mixing and weak stratification.

In contrast, Section CD shows both along-path reduction and pronounced vertical stratification. Salinity is ~24 near end C and gradually decreases to ~15.2-14.1 in the surface layer near end D. A clear two-layer structure develops in the mid-reach (~2-7 km), characterized by fresher surface water (≈16-17) extending seaward, overlying relatively saline bottom water (≈18-20) that forms a near-bed tongue/wedge, consistent with a halocline and salt-wedge feature.

Overall, the salinity structure is primarily controlled by freshwater input from the Paitan River and tidal dynamics. The river discharge (523.6 m³/s) supplies persistent low-salinity water and drives regional salinity gradients as well as the formation of salinity fronts/salt wedges. During peak flood, higher-salinity offshore water tends to intrude as a bottom layer into the semi-enclosed bay, whereas lighter freshwater preferentially occupies and spreads in the surface layer, maintaining the two-layer stratification along Section CD. By comparison, Section AB lies in shallow nearshore waters near the training dike, where strong tidal shear and bottom friction enhance turbulence, suppressing vertical salinity stratification; thus, salinity is expressed mainly as a sharp horizontal transition zone.

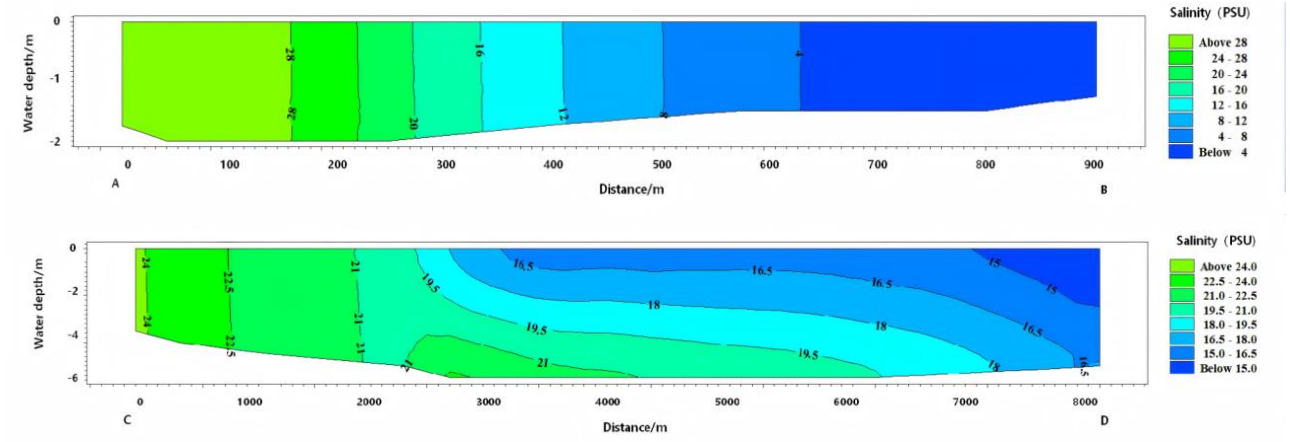

Fig. 6 Vertical salinity distributions along Sections AB and CD (PSU).

5.5 Coupled Temperature-Salinity-Density Features and Dispersion Mechanisms

Based on the vertical distributions of temperature, salinity, and density along Sections AB and CD, the water-mass structure along the dispersion pathway exhibits a transition from near-field mixing control to mid-far-field stratification control. At Section AB, the isolines of all three variables are nearly vertical, indicating strong vertical mixing and an almost homogeneous structure. The dominant processes are turbulent diffusion and rapid dilution, and the along-section decreases in temperature, salinity, and density occur concurrently, forming a sharp horizontal-gradient transition zone.

In contrast, Section CD shows a bay-scale two-layer configuration: low-salinity, low-density water spreads in the surface layer, while relatively high-salinity, high-density water advances near the bed, generating a stable halocline/pycnocline. Under this stratified background, the vertical temperature structure is also modulated, as evidenced by the curved and tilted isotherms in the mid-reach. This indicates that thermal dispersion is governed not only by tidal advection and engineering constraints, but also by freshwater-induced stratification and the resulting stable layering. Overall, the close correspondence between density and salinity suggests a representative coupling mechanism in which salinity primarily controls density, whereas temperature mainly modulates buoyancy in the study area.

6. Conclusions

This study investigated the winter thermal discharge from the Tianwan Nuclear Power Plant by developing a three-dimensional coupled numerical model. Model parameters were calibrated and validated against observed water levels, current speed/direction, and water temperature, demonstrating that the model can satisfactorily reproduce the hydrodynamic and thermal variability of the study area. On this basis, combined with the full-power discharge condition (total flow rate ≈ 500 m³/s and temperature rise ≈ 10 °C) and winter air-sea heat exchange (Ks ≈ 24.0 W m^{-2} $°C^{-1}$), we systematically analyzed the spatial extent of the 1-4 °C temperature-elevation zones and the planar, vertical-profile, and sectional characteristics of the temperature field.

The main findings are as follows:

(1) The vertical temperature gradient ranges from -0.34 to 1.10 °C/m and generally decreases with increasing distance from the outfall. The tidal-segment mean vertical temperature gradient from Stations #3 to #14 decreases from 0.18 °C/m to 0.08 °C/m.

(2) Vertical mixing is stronger during spring tides, whereas the mean vertical temperature gradient during neap tides is larger than that during spring tides by 0.02-0.17 °C/m. Along the main flow pathway, the planar temperature gradient is approximately 0.88-1.02 °C/km.

(3) A comparative analysis of Sections AB and CD indicates that the near field is dominated by strong

mixing and rapid dilution, while the mid-far field is jointly modulated by tidal transport, freshwater-induced stratification, and air-sea heat exchange. The dispersion exhibits a coupled mechanism in which salinity primarily controls density and temperature modulates buoyancy, providing scientific support for environmental impact assessment and optimization of thermal discharge management.

References

[1] Li, Y. L. 2022-06-21. "Promoting the 'Dual-Carbon' Goals through Comprehensive Utilization of Nuclear Energy." *People's Political Consultative Daily.*

[2] Liu, Y. Q., Zhou, J. S., Zhang, C. X., Sun, S. L., and Duan, M. N. 2022. "Impacts of Thermal Discharge from a Power Plant on Seawater Temperature and Zooplankton Community in Adjacent Waters." *Guangdong Chemical Industry* 49 (22): 105-8, 99.

[3] Ye, W. Q., Liu, H. R., Li, S. L., Liao, Y. P., Chen, Y., Tang, Y. B., Chen, Q. Z., Shou, L., and Du, P. 2021. "Long-Term Changes in the Ecological Environment of Coastal Waters Adjacent to the Qinshan Nuclear Power Plant." *Ocean Development and Management* 38 (9): 80-7.

[4] Li, M., Mo, Z. N., Lai, T. H., et al. Forthcoming. "Effects of Temperature Rise Induced by Thermal Discharge from a Coastal Power Plant on Mangrove Distribution and Expansion." *Guangxi Sciences.* (publication details to be completed)

[5] Muthulakshmi, A. L., Natesan, U., Ferrer, V. A., Deepthi, K., Venugopalan, V. P., and Narasimhan, S. V. 2019. "Impact Assessment of Nuclear Power Plant Discharge on Zooplankton Abundance and Distribution in Coastal Waters of Kalpakkam, India." *Ecological Processes* 8: 22.

[6] Jung, Y. H., Kim, H. J., and Park, H. S. 2018. "Thermal Discharge Effects on the Species Composition and Community Structure of Macrobenthos in the Rocky Intertidal Zone around the Taean Thermoelectric Power Plant, Korea." *Ocean and Polar Research* 40 (2): 59-67.

[7] Saravanan, P., Priya, A. M., Sundarakrishnan, B., Venugopalan, V. P., Rao, T. S., and Jayachandran, S. 2008. "Effects of Thermal Discharge from a Nuclear Power Plant on Culturable Bacteria at a Tropical Coastal Location in India." *Journal of Thermal Biology* 33 (7): 385-94.

[8] Arieli, R. N., Almogi-Labin, A., Abramovich, S., and Herut, B. 2011. "The Effect of Thermal Pollution on Benthic Foraminiferal Assemblages in the Mediterranean Shoreface Adjacent to Hadera Power Plant (Israel)." *Marine Pollution Bulletin* 62 (5): 1002-12.

[9] Zeng, Z., Luo, Y., Chen, Z. J., Tang, J. J., Wang, Y. H., and Chen, C. H. 2020. "Impact Assessment of Thermal Discharge from the Kemen Power Plant Based on Field Observation and Numerical Simulation." *Journal of Coastal Research* 104 (sp1): 351-61.

[10] Lowe, A. S., Schuepfer, F., and Dunning, J. D. 2009. "Case Study: Three-Dimensional Hydrodynamic Model of a Power Plant Thermal Discharge." *Journal of Hydraulic Engineering* 135 (4): 247-56.

[11] Tang, D. L., Kester, D. R., Wang, Z. D., Lian, J. S., Kawamura, H. 2003. "AVHRR Satellite Remote Sensing and Shipboard Measurements of the Thermal Plume from the Daya Bay Nuclear Power Station, China." *Remote Sensing of Environment* 84 (4): 506-15.

[12] Pan, C., Song, Z. K., Wang, R. S., and Fang, S. Q. 2024. "Study on the Impact of Thermal Discharge from the Sanmen Bay Power Plant on the Marine Environment." *Energy and Environment* 43 (6): 10-3.

[13] Chu, P. C., Fan, C. W., and Liu, W. T. 2000. "Determination of Vertical Thermal Structure from Sea Surface Temperature." *Journal of Atmospheric and Oceanic Technology* 17 (7): 971-9.

[14] Ni, P. T., Chen, P. X., and Huang, J. D. 2015. "Three-Dimensional Numerical Simulation of Thermal Diffusion of Thermal Discharge in the Yangxi Sea Area." *Guangdong Water Resources and Hydropower* 44 (6): 18-24.

[15] Chen, P. X., Huang, J. D., Ni, P. T., and Zhang, X. Y. 2012. "Numerical Simulation Study of Low-Level Radioactive Wastewater at the Hainan Changjiang Nuclear Power Plant." *Guangdong Water Resources and Hydropower* 41 (4): 17-9.